

# Survey-Wide Asteroid Discovery with a High-Performance Computing Enabled Non-Linear Digital Tracking Framework

Nathan Golovich<sup>a</sup>, Trevor Steil<sup>a</sup>, Alex Geringer-Sameth<sup>a</sup>, Keita Iwabuchi<sup>a</sup>, Ryan Dozier<sup>b</sup>, Roger Pearce<sup>a</sup>

<sup>a</sup>Lawrence Livermore National Laboratory, 7000 East Avenue, Livermore, 94550, California, United States of America

<sup>b</sup>University of Central Florida, 4328 Scorpius Street, Orlando, 32816, Florida, United States of America

## Abstract

Modern astronomical surveys detect asteroids by linking together their appearances across multiple images taken over time. This approach faces limitations in detecting faint asteroids and handling the computational complexity of trajectory linking. We present a novel method that adapts “digital tracking” - traditionally used for short-term linear asteroid motion across images - to work with large-scale synoptic surveys such as the Vera Rubin Observatory Legacy Survey of Space and Time (Rubin/LSST). Our approach combines hundreds of sparse observations of individual asteroids across their non-linear orbital paths to enhance detection sensitivity by several magnitudes. To address the computational challenges of processing massive data sets and dense orbital phase spaces, we developed a specialized high-performance computing architecture. We demonstrate the effectiveness of our method through experiments that take advantage of the extensive computational resources at Lawrence Livermore National Laboratory. This work enables the detection of significantly fainter asteroids in existing and future survey data, potentially increasing the observable asteroid population by orders of magnitude across different orbital families, from near-Earth objects (NEOs) to Kuiper belt objects (KBOs).

*Keywords:* Asteroid discovery, Synoptic Surveys, High-Performance Computing, Big Data

## 1. Introduction

Astronomical surveys that repeatedly image the sky with wide-field-of-view imagers offer the best chance to find minor planets. Astronomers typically detect moving objects in individual images and link them together across consecutive images on the basis of plausible trajectories. This method faces two primary challenges. First, the Solar System contains many minor planets, making it computationally expensive to link the correct detections without confusion, especially in very sensitive surveys. Second, since most minor planets are intrinsically very faint, astronomers must detect them on multiple images during the limited time spans when they are close to Earth. Exposures cannot be arbitrarily long, or sensitivity decreases due to trailing losses. To address these challenges, surveys use a strategy that allows astronomers to make and link repeat detections over minutes to days with enough precision for follow-up observations at other observatories.

Today, there are a handful of surveys that detect most asteroids, including the Catalina Sky Survey (CSS; Drake et al., 2009), the Panoramic Survey Telescope and Rapid Response System (Pan-STARRS; Chambers et al., 2016), and the Asteroid Terrestrial-impact Last Alert System (ATLAS; Tonry et al., 2018). Each of these surveys are geared toward detecting near-Earth objects (NEOs), which are minor planets (i.e., asteroids and comets) with perihelion less than 1.3 astronomical units

(AU). NEOs are the target for several dedicated surveys because their detection is the vital first step for planetary defense.

Other populations of asteroids remain further away from Earth, and thus pose no direct risk, but their study is scientifically useful for understanding Solar System formation and evolution and, indirectly, for planetary defense since all NEOs are sourced from further out in the Solar System before they enter orbits that bring them closer to Earth. These populations range from the main belt asteroids (MBAs) to the Kuiper belt objects (KBOs) and have been surveyed far less systematically across the Solar System. These objects are inherently fainter because of their larger distances, so longer exposures are required to detect them. However, all known objects move appreciably over time. For example, Sedna, among the farthest of the known minor planets, moves at  $\sim 0.3'' \text{ day}^{-1}$ .

In general, the farther out an object is, the longer is the time period over which its apparent motion can be approximated as linear. Motions may be approximated as linear across the sky for as long as a few weeks for KBOs and as long as a night for MBAs (see Figure 4 of Heinze et al., 2015). This approximately linear motion has been exploited to enable a simplified stacking procedure along parallel linear trajectories known colloquially as “digital tracking”, “synthetic tracking” or “track-before-detect”. The method has been used for about 20 years to study trans-Neptunian objects (TNOs; Tyson et al., 1992; Cochran et al., 1995; Bernstein et al., 2004; Whidden et al., 2019), MBAs (Heinze et al., 2015, 2019), and NEOs (Shao et al., 2014; Zhai et al., 2014, 2018, 2020; Lifset et al., 2021). Each of these examples of digital tracking methodologies have

*Email addresses:* golovich1@llnl.gov (Nathan Golovich), steil1@llnl.gov (Trevor Steil)

similar survey strategies: a spatially small survey composed of a dense stack of images spans a short period of time during which linear motion is a valid approximation. The signal-to-noise ratio (SNR) for image stacking scales as  $\sqrt{N}$ , where  $N$  is the number of exposures. Detection limits can therefore be pushed fainter by a few magnitudes for stacks of hundreds of exposures.

Over the next decade, the most prolific minor planet discovery engine will be the Vera C. Rubin Observatory Legacy Survey of Space and Time (LSST; Ivezic et al., 2008), which will observe the entire available night sky every few nights with six optical filters. Data will be automatically processed in real time, including the generation of difference images and automatic asteroid alerts (among other optical transients) as well as an automated asteroid detection and linking procedure (Juric et al., 2015; Heinze et al., 2022). The large aperture of the Rubin Observatory will deliver an unprecedented look into the orbital and luminosity distributions for all types of minor planets. The expected number of detected objects is  $5.5 \times 10^6$  MBAs,  $10^5$  NEOs,  $2.8 \times 10^5$  Jovian Trojans, and  $4 \times 10^4$  TNOs and KBOs (see Figure 5.1 of Abell et al., 2009). The typical asteroid will be detected hundreds of times over ten years (see Figure 5.4 of Abell et al., 2009).

This situation raises the question of whether or not these repeat observations can be used to enhance the sensitivity of LSST to even fainter solar system bodies. The basic idea is to view the hundreds of intersections between a minor planet’s orbit and LSST images similarly to the concept of digital tracking described above. The key difference is that digital tracking has only been used over short time spans<sup>1</sup> or those over which linear motion is a valid approximation. The ability to stack over years of imaging would translate to orders of magnitude more detections in surveys like LSST.

The challenge in doing so is computational. First, the generalization from linear motion to sky-projected orbital motion is complicated. Figure 1 shows the projected sky motion for various types of minor planets. Each of these curves is parametrized by six orbital elements and an orbital epoch. Geringer-Sameth et al. (in preparation) develops a general methodology to quantify density in the space of orbital elements as projected onto sky image data. They show that non-linear digital tracking searches are feasible for the outer Solar System with large high performance computing (HPC) systems. For linear digital tracking, an analogous calculation is presented in §2.3 of Heinze et al. (2015). Systematic searches for asteroids in the inner solar system are much more challenging with non-linear digital tracking. First, perturbations from the planets cause deviations from simple Keplerian motion over years-long surveys and must be accounted for. Second, the shorter distances mean that extremely small changes to orbital elements lead to detectable differences on the sky. The takeaway is that digital tracking in the non-linear regime should, at present, only be considered for minor planets beyond Jupiter.

<sup>1</sup>Bernstein et al. (2004) carried out a non-linear search for TNOs in stacks of 55 images taken over 5 days with the Hubble Space Telescope’s ACS camera.

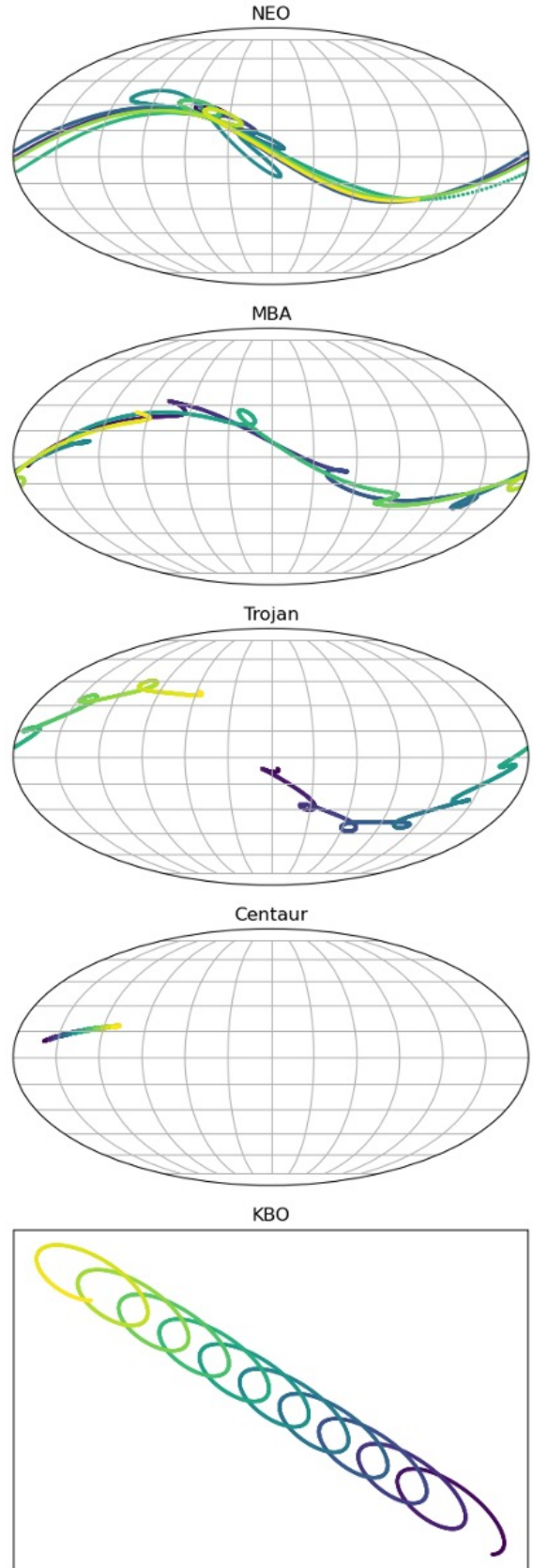


Figure 1: Projected sky motion over 10 years for minor planets from various populations ranging from the inner to outer Solar System. The color indicates time. For the KBO example, the object only moves only  $\sim 0.15$  deg over ten years. The helical looping is a parallax effect caused by Earth’s yearly motion around the sun while the broader trajectory is due to the minor planet’s motion.

Whether considering digital tracking in the linear or non-linear regime, the method is only as powerful as the number of individual image epochs that can be combined. Since the linear regime is bounded in the time domain, this forces experiments to gather data that are spatially narrow and dense in the time domain. All-sky synoptic surveys (such as LSST and the Zwicky Transient Facility, ZTF) are fundamentally different in that subsets of the data that are spatially narrow are necessarily sparse in the time domain (with the exception of the so-called deep drilling fields planned for LSST; [Abell et al., 2009](#)).

Combining the concept of digital tracking with synoptic surveys requires a novel computing architecture that can handle the sparse data intersections, large overall data volume, and extremely high required orbital phase space density. The features of such an architecture map well onto a number of computer science applications already deployed on HPC architectures, some of which have been explicitly developed to exploit the HPC architectures common at our place of work, Lawrence Livermore National Laboratory (LLNL). LLNL has long been home to cutting-edge HPC resources and at the time of writing, the world’s highest-performing HPC system is newly commissioned at LLNL ([Thomas, 2024](#)).

This paper describes the digital tracking framework we have built for asteroid detection using LLNL HPC systems. The remainder of this paper is organized as follows. In §2 we discuss the data that we use to develop and test our method. In §3 we discuss the computing framework that we assume for our method and how it influences the design of our algorithm. In §4 we present experiments using our algorithm to demonstrate performance. Finally in §5 we summarize our results and discuss the future development of our pipeline.

## 2. Data

LLNL was an institutional member of phase two of the Zwicky Transient Facility ([Bellm et al., 2019](#)). ZTF is an optical time-domain survey that uses the Palomar 48-inch Schmidt telescope. It has a  $47 \text{ deg}^2$  field of view and a 600 megapixel camera with an eight-second readout time. The survey is capable of imaging the northern sky at  $4000 \text{ deg}^2 \text{ hour}^{-1}$  to median depths of  $g \sim 20.8$  and  $r \sim 20.6$  (AB,  $5\sigma$  in 30 seconds). The camera is composed of 16 charge-coupled devices (CCDs), each with  $\sim 6000^2$  pixels. Each CCD outputs four quadrant files, which means that every image taken results in 64 files. For more details on the ZTF data reduction pipeline, we refer to [Masci et al. \(2019\)](#).

LLNL has a copy of all  $g$ ,  $r$  and  $i$ -band difference images produced by ZTF from March 2018 to February 2024, totaling  $\sim 400$  TB on disk and  $\sim 56$  million CCD quadrant files. Data are stored as `fpack` compressed FITS files ([Wells et al., 1981](#); [Pence et al., 2011](#)). ZTF data is available at <https://irsa.ipac.caltech.edu/Missions/ztf.html>.

## 3. Computing Framework

We designed our asteroid detection pipeline to leverage the power of modern heterogeneous computing architectures, using

the computational power of graphics processing units (GPUs) to intersect orbits with images, the storage capacity of node-local solid-state drives (SSDs) to provide fast access to massive partitioned data sets, and the low latency of HPC networks to coordinate between processes running on the system. Pseudocode for this pipeline is given in [Algorithm 1](#).

This framework specifically targets the Lassen supercomputer at LLNL<sup>2</sup>. Lassen contains 795 compute nodes, each of which features two IBM Power9 central processing units (CPUs) totaling 44 cores, four NVidia V100 GPUs each with 7.8 TFLOP/s of double precision performance and 16 GB of second-generation high bandwidth memory (HBM2), 256 GB of random access memory (RAM), a 1.2 TB SSD, and a dual-port Mellanox 100 Gb/s Infiniband network card. Although our work specifically targets Lassen, we have chosen to use libraries (discussed in §3.2) to make our code portable to new systems as they become available.

Our system starts by storing the relevant images for a given experiment on the SSDs available on each compute node. In order to maximize the number of images that can be handled, they are evenly partitioned across processes running on the set of available compute nodes without replication. When searching for asteroids, the CPUs sample sets of orbital parameters from specified distributions, with all CPUs being synchronized to sample the same orbits in the same order. These orbits are then transferred in batches to the GPUs which handle the non-linear tracking to determine which images are intersected by each orbit, and where within the relevant images those intersections occur. This step is a brute-force check of each (*image, orbit*) pair for intersections. We partition this computation across GPUs, so that each GPU is only considering intersections with the images that have been assigned to its compute node.

After we have found the set of intersections for the current batch of orbits, we filter the results to only contain those that are within the boundaries of an image. We transfer these compacted results from the GPU to the CPU, and for each valid intersection returned, a patch of pixels is pulled from the associated image on the node’s SSD. Each orbit is assigned a process that is responsible for assembling the results from individual processes running across the system to determine if an asteroid is present on the orbit. This communication of results is performed asynchronously by having processes send their valid results to the appropriate process as they are found.

The flow of data during asteroid detection is shown in [Figure 2](#). The GPU does the most floating-point intensive computations in order to determine where orbits intersect with images, taking the orbit parameters provided by the CPU and returning the locations of intersections. The CPU generates orbits used by the GPU, coordinates the collection of image data from the SSD for local image calculations, and sends its local results across the network to be combined with the results from other compute nodes in the system. The movement of data is all within a compute node except for the scatter and gather of the signal-to-noise (SNR) results from the images local to each

<sup>2</sup><https://hpc.llnl.gov/hardware/compute-platforms/lassen>

---

**Algorithm 1** Asteroid Search

---

**Input:** *image\_list*, *batch\_size*, *num\_batches***Output:** *DetectedObjects*

```
1: local_image_list  $\leftarrow$  PartitionImages(image_list) ▷ Assign images to processes
2: local_images, local_image_headers  $\leftarrow$  LoadImages(local_image_list) ▷ Read assigned images and extract header information
3: DetectedObjects  $\leftarrow$   $\emptyset$ 
4: for  $i \leftarrow 1$  to num_batches do
5:   orbits  $\leftarrow$  GenerateOrbits(batch_size)
6:   gpu_orbits  $\leftarrow$  CopyOrbitsToGPU(orbits)
7:   gpu_intersections  $\leftarrow$  SearchImages(gpu_orbits, local_image_headers) ▷ Dense  $|local\_images| \times |orbits|$  intersections
8:   filtered_intersections  $\leftarrow$  FilterGPUIntersections(gpu_intersections) ▷ Filter invalid intersections on GPU
9:   intersections  $\leftarrow$  CopyIntersectionsToHost(gpu_intersections)
10:  local_results  $\leftarrow$  FindLocalSignal(intersections, local_images)
11:  combined_results  $\leftarrow$  CommunicateResults(local_results)
12:  detections  $\leftarrow$  FindSignificantResults(combined_results)
13:  DetectedObjects  $\leftarrow$  DetectedObjects  $\cup$  detections
return DetectedObjects
```

---

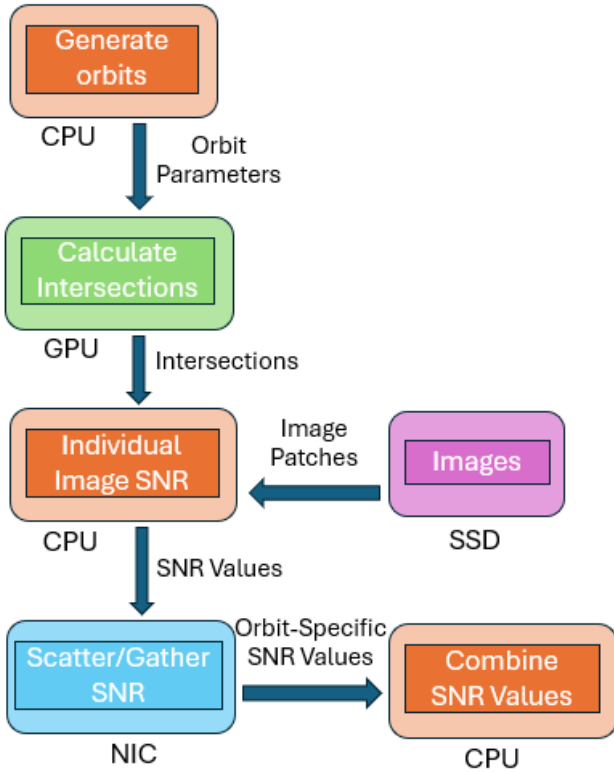


Figure 2: Flow of data within the asteroid detection pipeline. The CPU is largely in charge of coordinating the computation by sampling orbits that the GPU uses for the dense intersection calculations, pulling the appropriate portions of images from the node-local SSDs, and communicating individual-image signal-to-noise results (SNR) with processes on compute nodes across the system to determine if a detection was made.

compute node to the node assigned to the orbit. The assigned node makes the final determination of whether a candidate orbit contained an asteroid by jointly combining the signal from all intersections.

### 3.1. Computational Challenges

Searching for asteroids in data from telescope surveys presents many challenges, starting with the sheer amount of data that needs to be accessed, the limited amount of memory available on GPUs, the need to communicate sparse and irregular local results from individual processes to determine if a detection was made with a given set of orbital elements, and the desire for portable and performant code that can be utilized across HPC systems. The computational framework is guided by the constraints of the combination of these computational challenges.

#### 3.1.1. Data Volume

ZTF generates data at a rate of approximately 300 TB per year. In order to perform a meaningful survey of a population of possible asteroids, a significant portion of these images must be accessed. By holding these images on a parallel file system and accessing them as necessary, the rate at which images can be retrieved would be prohibitively too slow for this approach. To alleviate this bottleneck, we instead stage collections of images necessary for a family of orbits on the local SSDs of our systems, giving us significantly faster random access to individual images.

To improve the read performance, we tile images in smaller two-dimensional blocks as they are read from the parallel file system to each compute node’s SSD. This layout makes the pixels we need to gather from an image more likely to be on a small number of memory pages, reducing the bandwidth necessary to read a patch of an individual image. This differs from the standard page structure for FITS images.

Additionally, we *memory map* images on the node-local SSDs using the file-backed memory mapping technology (`mmap(2)` system call)<sup>3</sup>. By memory mapping, each image file is directly mapped to a region of the virtual memory space of the process and can be accessed as if it were being stored

<sup>3</sup>see <https://man7.org/linux/man-pages/man2/mmap.2.html>

on the main memory (DRAM) directly. This increases image data reading performance (higher bandwidth and lower latency) from the SSD by caching data on DRAM. This technique also has the benefit of delegating the complex data cache and transfer management from the application to the operating system (Van Essen et al., 2012).

### 3.1.2. GPU Memory

Testing large numbers of candidate orbits against a massive telescope survey data set requires large amounts of computing power, making this repeated calculation ideal for offloading onto a GPU. Each intersection operation requires converting the set of orbital parameters into a sky position at the time an image was taken, followed by converting these celestial coordinates to locations within the pixel grid of an image. The combination of these operations requires a few hundred bytes of data for each image, several tens of bytes for each orbit, and generates tens of bytes for each pair of image and candidate orbit. Orbits can be batched to reduce these costs, but when dealing with data sets containing millions of images on modern GPUs with access to tens of gigabytes of memory, these batches would be limited to single-digit sizes at the largest.

The orbital parameters associated with each batch of orbits require a transfer between the host and GPU. To increase the size of the data transferred at one time and reduce the effects of the latency of such transfers, batch sizes must be kept much larger. This pushes us to either partition images across compute nodes or stream image metadata from CPU to GPU. Given the frequent bottlenecks caused by the transfer of data to GPUs (Mohan et al., 2020; Leclerc et al., 2023), in this work we take the partitioning approach.

### 3.1.3. Communication of Results

After computing the intersection locations for a batch of orbits in the images partitioned throughout the system, each compute node holds a collection of partial results necessary to make a detection on individual orbits. These partial results held by an individual process are extremely sparse, as the probability is very low for a random orbit to intersect any of the thousands of images a particular process is responsible for.

The sparsity of results leads to an “all-to-many” communication pattern. Each process has results to communicate and receive, and an individual process is only going to communicate with a small but non-trivial subset of processes in the system. In order to handle these irregular communication patterns, we make use of YGM (Steil et al., 2023), an asynchronous communication library designed for these types of all-to-many patterns in HPC. In this setting, processes independently assemble the local results from the images available and then asynchronously send these results to their destination. At the destination, the local results are assembled into a global assessment of a particular orbit once all local results have been received. This asynchronous method of computing allows individual processes to begin combining the partial results from other processes as they become available without having to wait for all other processes to finish communication before starting.

### 3.2. Performance Portability

When writing scientific software, runtimes and programming models can be utilized to achieve high performance on available HPC systems. These techniques often tie a project to specific hardware. The true desire is the ability to run scientific software on a variety of systems without maintaining versions of code for every architecture being targeted, while also achieving close to optimal performance.

Multiple performance portability solutions are available to make these conflicting goals more attainable. Kokkos is a C++ performance portability library (Carter Edwards et al., 2014) that uses the abstraction of execution spaces and memory spaces to specify the physical hardware on which the code will run and where a piece of data resides on the various memory devices available to a system. RAJA (Beckingsale et al., 2019) is a similar performance portability library that abstracts computation from the architecture but allows users to more explicitly control details such as memory management and memory access patterns.

In our case, we want to run on different systems based on the amount of available RAM and SSD space while making use of any accelerators present for the floating point-intensive intersection calculations. We chose to use the RAJA performance portability library for its ability to express loop-level parallelism that can be run on CPUs and multiple accelerators, while being easy to integrate with existing code and libraries. This allows us to write computationally intensive portions of code using RAJA to be offloaded to accelerators while being free to use YGM to handle the communication in our algorithm, as described in §3.1.3.

## 4. Experimental Results

For testing of our HPC asteroid detection pipeline, we use LLNL’s Lassen supercomputer described in §3. As a system, Lassen showcases the heterogeneous architecture with performant GPUs for compute-intensive orbit intersection calculations, node-local SSDs for storing large image data sets, and a high-bandwidth network for coordination of the results spread across each processor in the system.

### 4.1. Verification Studies

In order to verify that our HPC asteroid detection pipeline is producing correct results, we perform verification studies comparing to results obtained from an asteroid detection pipeline separately developed in Python. This Python implementation uses SSAPy<sup>4</sup> (Yeager et al., 2023; Schlafly et al., 2023) to propagate orbits in time and *astropy*<sup>5</sup> (Astropy Collaboration et al., 2013, 2018, 2022) to determine the pixel coordinates of intersections between orbits and images. It has been extensively tested against JPL Horizons<sup>6</sup> (Giorgini, 2011) and bright asteroids in ZTF. We used the Python implementation to verify the HPC pipeline’s predicted location of intersections and final signal-to-noise ratio of detections.

<sup>4</sup><https://github.com/LLNL/SSAPy>

<sup>5</sup>*astropy*’s WCS implementation is based on WCSLIB (Calabretta, 2011).

<sup>6</sup><https://ssd.jpl.nasa.gov/horizons>

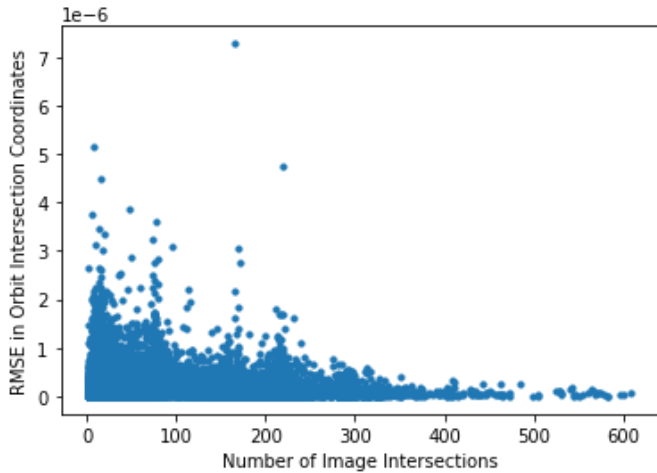


Figure 3: RMSE for asteroid pixel coordinates within intersected images compared to calculations using SSAPy and astropy.

#### 4.1.1. Intersection Location Verification

For intersection verification of our HPC detection pipeline, we compare with the Python implementation across a collection of sampled orbits. For this experiment, we tested a collection of 24486 randomly sampled orbits against two million images from the ZTF data set. Of these 24486 orbits, 21618 intersected at least one of the images used, giving 1.81 million total intersections.

We compare our implementations using the root mean square error (RMSE) of intersections in pixels for an individual orbit, calculated as

$$\text{RMSE} = \sqrt{\frac{1}{N} \sum_{i=1}^N \|X_i - \hat{X}_i\|_2^2}$$

where the  $X_i$  are the intersection locations in pixel space as given by Python and the  $\hat{X}_i$  are the intersection locations determined by the HPC pipeline. Figure 3 shows the RMSE for each orbit, separated by the number of intersections given by each orbit. We can see most error values clustered around zero, with the largest errors approaching  $10^{-5}$  pixels.

#### 4.1.2. Detection Verification

For detection verification, we compare with the Python implementation for detecting the Centaur (2060) Chiron. In this setting, we perturb the semi-major axis of Chiron’s orbit as specified by the Horizons system<sup>7</sup> to compare in the cases of true detections and misses. Figure 4 shows the signal-to-noise ratio of both implementations in this setting, exhibiting strong agreement between the two.

#### 4.2. Performance Studies

For applications of our non-linear digital tracking framework, we are often limited by the amount of imagery data that

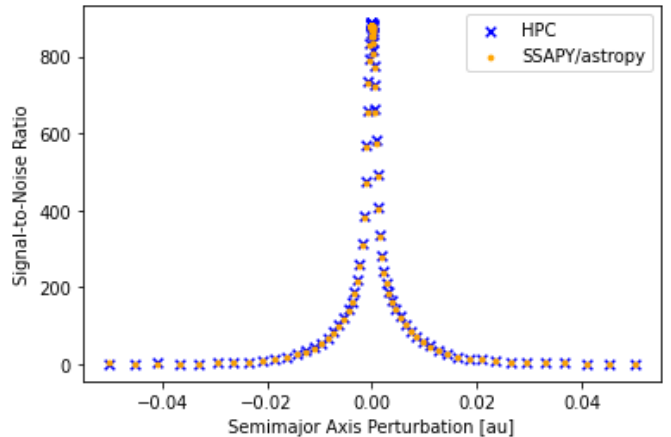


Figure 4: Signal-to-noise ratio of HPC and SSAPy/astropy asteroid detection pipelines for orbits based on a known object (Chiron) with perturbed semi-major axis values.

can be held at one time. Using four bytes per pixel, an image from ZTF takes 36 MB of space. For each terabyte of local SSD space available for storing images, we can store just over 29,000 images, much fewer than the 10s of millions of image files that comprise the ZTF survey. Weak scaling studies in which each compute node is given the most data possible are the most relevant given the combination of data set sizes and our intended use case. In this setting, it is worth noting that for a given set of orbits to search, doubling the number of images being tested against also roughly doubles the amount of computation required, as each orbit is intersected with all available images.

For these performance studies, we loaded 20,000 images on the SSDs attached to each compute node and tested 1.3 million orbits for detections within the available images. We focus on two separate test cases. The first is a diffuse search where a broad swath of images and orbits are used. This case is representative of a blind search for unknown asteroids. The second is a focused search in which a smaller class of orbits with a large semi-major axis is tested against a set of images chosen to be located in the direction of this collection of orbits. The parameters chosen for this focused search are based on the set of parameters identified as candidate orbits of the hypothesized planet Nine (Batygin et al., 2019; Brown and Batygin, 2021, 2022).

The results of our weak-scaling study in which each compute node has the same number of images assigned regardless of the number of compute nodes are given in Figure 5. In this setting, each GPU in the system is performing the same amount of work as the number of nodes increases because we are using a fixed number of orbits and the number of images per compute node remains constant. In the bottom of Figure 5, note that the number of intersections between candidate orbits and the set of images scales linearly with the number of compute nodes. This quantity reflects the amount of intersection data that must be transferred from the GPU to the host, as well as the number of images that are required to be read from each SSD. As this

<sup>7</sup><https://ssd.jpl.nasa.gov/horizons>

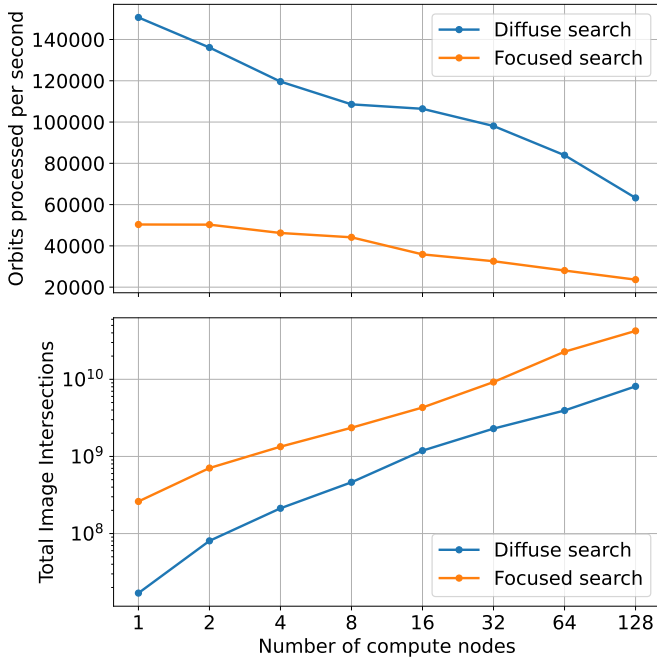


Figure 5: Weak scaling results for asteroid detection pipeline for focused and diffuse search cases including total throughput (top) and number of intersections processed (bottom) in each setting.

scales linearly with the number of compute nodes, the amount of work being performed by each compute node remains relatively constant as the scale of the problem is increased.

Despite this fixed amount of work that each compute node performs, the top of Figure 5 shows that the system throughput slowly degrades with increasing numbers of compute nodes. This effect is largely due to variations in the number of valid intersections that any rank finds within a given batch of orbits. Each intersection requires pixel values to be retrieved from the node-local SSDs, which is a relatively costly operation. Our performance in this phase of the calculation is largely bound by the slowest processor in the system. As the number of compute nodes is increased, the chance that a compute node identifies an outlier in the number of valid image intersections increases.

The above effect is highlighted in Figure 6. The figure shows the maximum number of valid intersections found by any rank across the 8000 orbits in a batch. On one compute node, averaged over 1024 batches of orbits, this maximum number is 30.2, while on 128 compute nodes it increases to 91.1. The effect of this on the time required to retrieve pixels is shown in Table 1. The results shown were taken from a diffuse search experiment. The intersections were calculated on the GPUs, and the pixels were retrieved from images stored on the SSDs, but the results were not communicated to compute a final detection. This was done to isolate the amount of time that was spent waiting for the data from the SSDs. The time to retrieve pixels approximately quadrupled between one compute node and 128 compute node experiments. This is due to the tripling in the maximum number of valid intersections calculated in each batch when scaling across the same number of compute nodes.

In Table 1, we show a 55% increase in the total run time

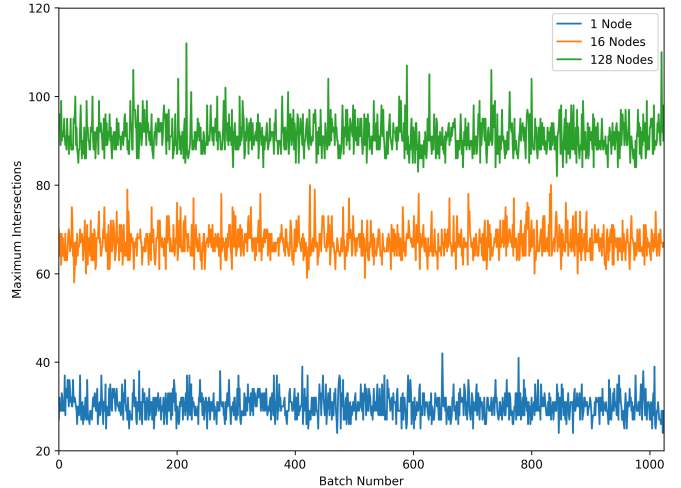


Figure 6: Maximum number of valid intersections identified on any individual MPI rank across 8000 orbits each for a blind search survey experiment. Results are shown for 1024 example batches of orbits run on different numbers of compute nodes.

Compute Nodes	Intersection Time (sec)	Pixel Retrieval Time (sec)	Total Time (sec)
1	44.33	9.31	53.64
2	45.92	7.78	53.70
4	45.11	17.33	62.44
8	44.89	17.21	62.10
16	45.04	18.39	63.43
32	46.86	22.02	67.88
64	46.14	29.48	75.62
128	45.71	37.37	83.08

Table 1: Amount of time needed for calculating intersections between images and orbits and retrieving pixels from images (without communicating results) in a diffuse search setting.

when scaling from 1 to 128 compute nodes. This is due to an increase in the time spent retrieving pixels. This corresponds to a roughly 35% decrease in total throughput, which accounts for most of the performance degradation seen in Figure 5.

This scalability could likely be addressed by combining multiple batches of intersections found on the GPU in our current approach as mini-batches of much larger batches that the CPU manages. This approach will allow variations within mini-batches to average out across multiple batches and bring outliers to lower levels as we scale to more compute nodes. In our case, we cannot simply increase the batch size the GPU is processing due to memory constraints on the GPUs.

## 5. Discussion

### 5.1. Summary

We have presented a non-linear digital tracking pipeline that utilizes HPC systems to search for asteroids over timescales in which asteroid motion is highly non-linear. This system makes

use of the following features available with many modern clusters:

- the massive parallelism created by graphics processing units (GPUs) to propagate large numbers of candidate orbits and detect intersections with large imagery data sets,
- high-speed networks to coordinate intermediate results between processors in the system, and
- node-local storage on compute nodes to access very large image data sets with lower latency and higher bandwidth compared to parallel file systems.

By propagating orbits through such large data sets, we are able to combine the signal present in relatively large numbers of images. This increases the signal-to-noise ratio and allows for fainter detections to be made.

We perform multiple experiments to demonstrate the accuracy and scalability of our pipeline. We compare results with a trusted implementation using `SSAPy` and `astropy` to validate intersections with individual images, as well as SNR values for entire orbits. We have demonstrated the scalability of this approach to tackle data sets containing millions of images using up to 128 nodes on the Lassen cluster. Increasing the scale of the data set and cluster allocation is associated with a small decrease in total system throughput.

## 5.2. Future Work

### 5.2.1. Reduce Local Storage Requirements

In our current implementation, images are partitioned across the local storage residing on each compute node. This allows us to maintain fast random access to all images simultaneously, eliminating the bottleneck of retrieving images from the parallel file system as needed.

This approach requires an allocation of compute nodes that is large enough to hold the entire data set. By partitioning the set of orbits to sample from, we could potentially reduce the portion of the data set needed at any one time, allowing a large data set to be searched with a smaller allocation of compute nodes.

### 5.2.2. Improve Performance and Scalability

As shown in Figure 5, the rate at which we can process sampled orbits slowly declines as we increase the number of compute nodes used and the number of images being searched, giving roughly 40% of the throughput at 128 compute nodes as on a single compute node. Maintaining the same throughput while scaling the problem size and compute resources is often not a reasonable goal, but our scalability could likely be improved.

Our current implementation handles image intersections on the GPUs and the lookup of pixel values within images as distinct steps. In a pipelined implementation, we would use the GPUs to begin calculating intersections for the next batch of sampled orbits while the pixels within images are being retrieved for the current batch of orbits. Pipelining is a commonly used optimization technique that has been applied to the problems of scheduling operations within loops (Allan et al., 1995),

hiding data transfer times on heterogeneous architectures to optimize matrix operations (Wang et al., 2011), and optimizing deep neural network training on multiple accelerators (Huang et al., 2019). In the context of asteroid detection, pipelining would improve performance at all scales by allowing CPUs and GPUs to work simultaneously, and it may improve the scalability by alleviating some of the effects of work imbalance within batches of orbits by removing additional synchronization points.

In addition to pipelining, decoupling the batch sizes used on the GPU and CPU can likely improve the throughput of our non-linear digital tracking framework, as discussed in Section 4.2. Our current batch size is limited by the amount of memory available on GPUs, but this relatively small batch size leads to individual processes finding significantly larger numbers of valid intersections than the average process. Treating several mini-batches of GPU orbits as a single larger batch of orbits on the CPU would lower this variance and improve scalability.

### 5.2.3. Interpretation of Detection Results

The HPC non-linear digital tracking pipeline presented in this paper is able to handle data sets with millions of images and process tens of thousands of orbits per second. This is able to produce large numbers of detections above an SNR of 5, but most of these are false positives caused by chance alignment of correlated noise across images due to imperfect difference image generation. We are continuing to work to filter these spurious detections quickly to identify the true detections resulting from our searches. A simple masking procedure around stars from the Gaia catalog (Gaia Collaboration et al., 2016) or Pan-STARRS (Flewelling et al., 2020) appears to remove the vast majority of false positives. A more sophisticated method is to identify outliers among individual intersection SNR calculations. The relative SNR of an intersection can be predicted based on the noise level, zero point, and geometry of the Sun, Earth, asteroid configuration. Intersections with anomalously high SNR value compared to the expectation can be removed. We are also exploring filtering with supervised learning methods based on training a neural network to recognize prepared image stacks of false positives and true positives. After filtering, the remaining detections above the threshold are few, and a coordinated follow-up program with a large telescope can confirm discoveries. Regardless of which method is used, the false positive rate will ultimately need to be quantified so that detections can be contextualized.

Another challenge in handling detections with this method is the difficulty of confirming detections without follow-up observations. We aim to use this method to detect minor planets in the outer Solar System. KBOs, for example, are important tracers of Solar System formation processes, so any detection will be worthy of dedicated follow-up observations to confirm. For larger scale surveys with our method, population studies can be carried out by injecting fake sources and estimating the recovery rate. Then, lists of detections can be used to estimate the population under the orbital distribution that was searched (e.g. Bernstein et al., 2004; Fraser and Kavelaars, 2009; Morbidelli et al., 2021).

#### 5.2.4. Porting to El Capitan Systems

El Capitan is the newest exascale Department of Energy supercomputer sited at Lawrence Livermore National Laboratory (Thomas, 2024). El Capitan features over 11,000 compute nodes equipped with AMD MI300A accelerated processing unit (APU) chips. These APUs are each composed of a set of CPU cores tightly coupled to three GPU chips. These CPU and GPU cores share 512 GB of high-bandwidth memory (HBM) resources, allowing direct access to memory from the CPU and GPU cores. This unified memory allows computations to proceed without expensive data transfers between CPUs and GPUs, alleviating many memory bottlenecks. In addition to computing resources, El Capitan’s nodes are attached to near-node storage appliances called Rabbits (Auten and Eperly, 2023). These Rabbits allow storage of large telescope surveys on fast local storage, much like the SSDs found on the compute nodes of Lassen.

Porting our asteroid detection pipeline to the El Capitan architecture is of great interest and has been planned for in our choice to use the RAJA performance portability library, as outlined in Section 3.2. The techniques for improving scalability discussed in Section 5.2.2 are specifically targeted at the Lassen architecture, centering around the limited availability of memory on discrete GPUs. The hardware on El Capitan does not face the same limitations because the GPU resources have access to each compute node’s full 512 GB of HBM, a large improvement over the 64 GB of total HBM available to GPUs on each compute node of Lassen. This increased availability of memory would allow much larger batches of orbits to be tested on El Capitan systems.

Having access to the same memory space on CPUs and GPUs would allow the use of more standard producer-consumer queues in which individual compute resources operate on their data and place the results in a queue for the hardware that handles the next computational step. This would allow CPUs and GPUs to operate without explicit synchronization. Additional optimizations could be incorporated depending on the relative lengths of the work queues, such as GPUs performing additional reorganization of the valid intersections found to put them in an order more likely to yield reuse of imagery data by the CPU. Such an optimization would be especially fruitful given the larger batches of orbits that GPUs could process on El Capitan systems compared to Lassen.

These potential improvements from new APU systems could likely further improve the performance of our non-linear digital tracking framework. With its ability to process data sets that contain millions of images, we believe that this framework could be a powerful tool for minor planet detection.

#### Acknowledgments

This work was performed under the auspices of the U.S. Department of Energy by Lawrence Livermore National Laboratory under Contract DE-AC52-07NA27344. This work was supported by the Lawrence Livermore National Laboratory LDRD Program under Project 2023-ERD-044. The LLNL document number is LLNL-JRNL-872678.

This work was based on observations obtained with the Samuel Oschin Telescope 48-inch and the 60-inch Telescope at the Palomar Observatory as part of the Zwicky Transient Facility project. ZTF is supported by the National Science Foundation under Grants No. AST-1440341 and AST-2034437 and a collaboration including current partners Caltech, IPAC, the Oskar Klein Center at Stockholm University, the University of Maryland, University of California, Berkeley, the University of Wisconsin at Milwaukee, University of Warwick, Ruhr University, Cornell University, Northwestern University and Drexel University. Operations are conducted by COO, IPAC, and UW.

#### References

- Abell, P.A., Allison, J., Anderson, S.F., Andrew, J.R., Angel, J.R.P., Armus, L., Arnett, D., Asztalos, S.J., Axelrod, T.S., Bailey, S., et al., 2009. Lsst science book, version 2.0 [arXiv:0912.0201](https://arxiv.org/abs/0912.0201).
- Allan, V.H., Jones, R.B., Lee, R.M., Allan, S.J., 1995. Software pipelining. *ACM Comput. Surv.* 27, 367432. URL: <https://doi.org/10.1145/212094.212131>, doi:10.1145/212094.212131.
- Astropy Collaboration, Price-Whelan, A.M., Lim, P.L., Earl, N., Starkman, N., Bradley, L., Shupe, D.L., Patil, A.A., Corrales, L., Brasseur, C.E., N’othe, M., Donath, A., Tollerud, E., Morris, B.M., Ginsburg, A., Vaher, E., Weaver, B.A., Tocknell, J., Jamieson, W., van Kerkwijk, M.H., Robitaille, T.P., Merry, B., Bachetti, M., G’unter, H.M., Aldcroft, T.L., Alvarado-Montes, J.A., Archibald, A.M., B’odi, A., Bapat, S., Barentsen, G., Baz’an, J., Biswas, M., Boquien, M., Burke, D.J., Cara, D., Cara, M., Conroy, K.E., Conseil, S., Craig, M.W., Cross, R.M., Cruz, K.L., D’Eugenio, F., Dencheva, N., Devillepoix, H.A.R., Dietrich, J.P., Eigenbrot, A.D., Erben, T., Ferreira, L., Foreman-Mackey, D., Fox, R., Freij, N., Garg, S., Geda, R., Glatly, L., Gondhalekar, Y., Gordon, K.D., Grant, D., Greenfield, P., Groener, A.M., Guest, S., Gurovich, S., Handberg, R., Hart, A., Hatfield-Dodds, Z., Homeier, D., Hosseinzadeh, G., Jenness, T., Jones, C.K., Joseph, P., Kalmbach, J.B., Karamahmetoglu, E., Kaluszynski, M., Kelley, M.S.P., Kern, N., Kerzendorf, W.E., Koch, E.W., Kulumani, S., Lee, A., Ly, C., Ma, Z., MacBride, C., Maljaars, J.M., Muna, D., Murphy, N.A., Norman, H., O’Steen, R., Oman, K.A., Pacifici, C., Pascual, S., Pascual-Granado, J., Patil, R.R., Perren, G.I., Pickering, T.E., Rastogi, T., Roulston, B.R., Ryan, D.F., Rykoff, E.S., Sabater, J., Sakurikar, P., Salgado, J., Sanghi, A., Saunders, N., Savchenko, V., Schwardt, L., Seifert-Eckert, M., Shih, A.Y., Jain, A.S., Shukla, G., Sick, J., Simpson, C., Singanamalla, S., Singer, L.P., Singhal, J., Sinha, M., SipHocz, B.M., Spitler, L.R., Stansby, D., Streicher, O., Sumak, J., Swinbank, J.D., Taranu, D.S., Tewary, N., Tremblay, G.R., Val-Borro, M.d., Van Kooten, S.J., Vasovi’c, Z., Verma, S., de Miranda Cardoso, J.V., Williams, P.K.G., Wilson, T.J., Winkel, B., Wood-Vasey, W.M., Xue, R., Yoachim, P., Zhang, C., Zonca, A., Astropy Project Contributors, 2022. The Astropy Project: Sustaining and Growing a Community-oriented Open-source Project and the Latest Major Release (v5.0) of the Core Package. *ApJ* 935, 167. doi:10.3847/1538-4357/ac7c74, [arXiv:2206.14220](https://arxiv.org/abs/2206.14220).
- Astropy Collaboration, Price-Whelan, A.M., Sip’ocz, B.M., G’unter, H.M., Lim, P.L., Crawford, S.M., Conseil, S., Shupe, D.L., Craig, M.W., Dencheva, N., Ginsburg, A., VanderPlas, J.T., Bradley, L.D., P’erez-Su’arez, D., de Val-Borro, M., Aldcroft, T.L., Cruz, K.L., Robitaille, T.P., Tollerud, E.J., Ardelean, C., Babej, T., Bach, Y.P., Bachetti, M., Bakanov, A.V., Bamford, S.P., Barentsen, G., Barmby, P., Baumbach, A., Berry, K.L., Biscani, F., Boquien, M., Bostroem, K.A., Bouma, L.G., Brammer, G.B., Bray, E.M., Breytenbach, H., Buddelmeijer, H., Burke, D.J., Calderone, G., Cano Rodr’iguez, J.L., Cara, M., Cardoso, J.V.M., Cheedella, S., Copin, Y., Corrales, L., Crichton, D., D’Avella, D., Deil, C., Depagne, ’E., Dietrich, J.P., Donath, A., Droettboom, M., Earl, N., Erben, T., Fabbro, S., Ferreira, L.A., Finethy, T., Fox, R.T., Garrison, L.H., Gibbons, S.L.J., Goldstein, D.A., Gommers, R., Greco, J.P., Greenfield, P., Groener, A.M., Grullier, F., Hagen, A., Hirst, P., Homeier, D., Horton, A.J., Hosseinzadeh, G., Hu, L., Hunkeler, J.S., Ivezi’c, ’Z., Jain, A., Jenness, T., Kanarek, G., Kendrew, S., Kern, N.S., Kerzendorf, W.E., Khvalko, A., King, J., Kirkby, D., Kulkarni, A.M., Kumar, A., Lee, A., Lenz, D., Littlefair, S.P., Ma, Z., Macleod, D.M., Mastropietro, M., McCully, C., Montagnac, S., Morris, B.M., Mueller, M.,

- Mumford, S.J., Muna, D., Murphy, N.A., Nelson, S., Nguyen, G.H., Nínan, J.P., Nöthe, M., Ogaz, S., Oh, S., Parejko, J.K., Parley, N., Pascual, S., Patil, R., Patil, A.A., Plunkett, A.L., Prochaska, J.X., Rastogi, T., Reddy Janga, V., Sabater, J., Sakurikar, P., Seifert, M., Sherbert, L.E., Sherwood-Taylor, H., Shih, A.Y., Sick, J., Silbiger, M.T., Singanamalla, S., Singer, L.P., Sladen, P.H., Sooley, K.A., Sornarajah, S., Streicher, O., Teuben, P., Thomas, S.W., Tremblay, G.R., Turner, J.E.H., Terrón, V., van Kerkwijk, M.H., de la Vega, A., Watkins, L.L., Weaver, B.A., Whitmore, J.B., Woillez, J., Zabalza, V., *Astropy* Contributors, 2018. The *Astropy* Project: Building an Open-science Project and Status of the v2.0 Core Package. *AJ* 156, 123. doi:[10.3847/1538-3881/aabc4f](https://doi.org/10.3847/1538-3881/aabc4f), [arXiv:1801.02634](https://arxiv.org/abs/1801.02634).
- Astropy* Collaboration, Robitaille, T.P., Tollerud, E.J., Greenfield, P., Droettboom, M., Bray, E., Aldcroft, T., Davis, M., Ginsburg, A., Price-Whelan, A.M., Kerzendorf, W.E., Conley, A., Crighton, N., Barbary, K., Muna, D., Ferguson, H., Grollier, F., Parikh, M.M., Nair, P.H., Unther, H.M., Deil, C., Woillez, J., Conseil, S., Kramer, R., Turner, J.E.H., Singer, L., Fox, R., Weaver, B.A., Zabalza, V., Edwards, Z.I., Azalee Bostroem, K., Burke, D.J., Casey, A.R., Crawford, S.M., Dencheva, N., Ely, J., Jenness, T., Labrie, K., Lim, P.L., Pierfederici, F., Pontzen, A., Ptak, A., Refsdal, B., Servillat, M., Streicher, O., 2013. *Astropy*: A community Python package for astronomy. *A&A* 558, A33. doi:[10.1051/0004-6361/201322068](https://doi.org/10.1051/0004-6361/201322068), [arXiv:1307.6212](https://arxiv.org/abs/1307.6212).
- Auten, H., Epperly, M., 2023. Road to El Capitan 4: Storage in the exascale era. <https://computing.llnl.gov/about/newsroom/road-el-capitan-4>.
- Batygin, K., Adams, F.C., Brown, M.E., Becker, J.C., 2019. The planet nine hypothesis. *Physics Reports* 805, 1–53.
- Beckingsale, D.A., Burmark, J., Hornung, R., Jones, H., Killian, W., Kunen, A.J., Pearce, O., Robinson, P., Ryujin, B.S., Scogland, T.R., 2019. Raja: Portable performance for large-scale scientific applications, in: 2019 IEEE/ACM International Workshop on Performance, Portability and Productivity in HPC (P3HPC), IEEE. pp. 71–81.
- Bellm, E.C., Kulkarni, S.R., Graham, M.J., Dekany, R., Smith, R.M., Riddle, R., Masci, F.J., Helou, G., Prince, T.A., Adams, S.M., Barbarino, C., Barlow, T., Bauer, J., Beck, R., Belicki, J., Biswas, R., Blagorodnova, N., Bodewits, D., Bolin, B., Brinell, V., Brooke, T., Bue, B., Bulla, M., Burrows, R., Cenko, S.B., Chang, C.K., Connolly, A., Coughlin, M., Cromer, J., Cunningham, V., De, K., Delacroix, A., Desai, V., Duev, D.A., Eadie, G., Farnham, T.L., Feeney, M., Feindt, U., Flynn, D., Franckowiak, A., Frederick, S., Fremling, C., Gal-Yam, A., Gezari, S., Giomi, M., Goldstein, D.A., Golkhou, V.Z., Goobar, A., Groom, S., Hacopians, E., Hale, D., Henning, J., Ho, A.Y.Q., Hover, D., Howell, J., Hung, T., Huppenkothen, D., Imel, D., Ip, W.H., Ivezić, Ž., Jackson, E., Jones, L., Juric, M., Kasliwal, M.M., Kaspi, S., Kaye, S., Kelley, M.S.P., Kowalski, M., Kramer, E., Kupfer, T., Landry, W., Laher, R.R., Lee, C.D., Lin, H.W., Lin, Z.Y., Lunnan, R., Giomi, M., Mahabal, A., Mao, P., Miller, A.A., Monkewitz, S., Murphy, P., Ngeow, C.C., Nordin, J., Nugent, P., Ofek, E., Patterson, M.T., Penprase, B., Porter, M., Rauch, L., Rebbapragada, U., Reiley, D., Rigault, M., Rodriguez, H., van Roestel, J., Rusholme, B., van Santen, J., Schulze, S., Shupe, D.L., Singer, L.P., Soumagnac, M.T., Stein, R., Surace, J., Sollerman, J., Szkody, P., Taddia, F., Terek, S., Van Stintne, A., van Velzen, S., Vestrand, W.T., Walters, R., Ward, C., Ye, Q.Z., Yu, P.C., Yan, L., Zolkower, J., 2019. The Zwicky Transient Facility: System Overview, Performance, and First Results. *PASP* 131, 018002. doi:[10.1088/1538-3873/aaecbe](https://doi.org/10.1088/1538-3873/aaecbe), [arXiv:1902.01932](https://arxiv.org/abs/1902.01932).
- Bernstein, G.M., Trilling, D.E., Allen, R.L., Brown, M.E., Holman, M., Malhotra, R., 2004. The Size Distribution of Trans-Neptunian Bodies. *AJ* 128, 1364–1390. doi:[10.1086/422919](https://doi.org/10.1086/422919), [arXiv:astro-ph/0308467](https://arxiv.org/abs/astro-ph/0308467).
- Brown, M.E., Batygin, K., 2021. The orbit of planet nine. *The Astronomical Journal* 162, 219.
- Brown, M.E., Batygin, K., 2022. A search for planet nine using the Zwicky Transient Facility public archive. *The Astronomical Journal* 163, 102.
- Calabretta, M.R., 2011. Wcslib and Pgsbox. *Astrophysics Source Code Library*, record ascl:1108.003.
- Carter Edwards, H., Trott, C.R., Sunderland, D., 2014. Kokkos: Enabling manycore performance portability through polymorphic memory access patterns. *Journal of Parallel and Distributed Computing* 74, 3202–3216. URL: <https://www.sciencedirect.com/science/article/pii/S0743731514001257>, doi:<https://doi.org/10.1016/j.jpdc.2014.07.003>. domain-Specific Languages and High-Level Frameworks for High-Performance Computing.
- Chambers, K.C., Magnier, E.A., Metcalfe, N., Flewelling, H.A., Huber, M.E., Waters, C.Z., Denneau, L., Draper, P.W., Farrow, D., Finkbeiner, D.P., Holmberg, C., Koppenhoefer, J., Price, P.A., Rest, A., Saglia, R.P., Schlafly, E.F., Smartt, S.J., Sweeney, W., Wainscoat, R.J., Burgett, W.S., Chastel, S., Grav, T., Heasley, J.N., Hodapp, K.W., Jedicke, R., Kaiser, N., Kudritzki, R.P., Luppino, G.A., Lupton, R.H., Monet, D.G., Morgan, J.S., Onaka, P.M., Shiao, B., Stubbs, C.W., Tonry, J.L., White, R., Bañados, E., Bell, E.F., Bender, R., Bernard, E.J., Boegner, M., Boffi, F., Botticella, M.T., Calamida, A., Casertano, S., Chen, W.P., Chen, X., Cole, S., Deacon, N., Frenk, C., Fitzsimmons, A., Gezari, S., Gibbs, V., Goessl, C., Goggia, T., Gourgue, R., Goldman, B., Grant, P., Grebel, E.K., Hambly, N.C., Hasinger, G., Heavens, A.F., Heckman, T.M., Henderson, R., Henning, T., Holman, M., Hopp, U., Ip, W.H., Isani, S., Jackson, M., Keyes, C.D., Koekemoer, A.M., Kotak, R., Le, D., Liska, D., Long, K.S., Lucey, J.R., Liu, M., Martin, N.F., Masci, G., McLean, B., Mindel, E., Misra, P., Morganson, E., Murphy, D.N.A., Obaika, A., Narayan, G., Nieto-Santesteban, M.A., Norberg, P., Peacock, J.A., Pier, E.A., Postman, M., Primak, N., Rae, C., Rai, A., Riess, A., Riffeser, A., Rix, H.W., Röser, S., Russel, R., Rutz, L., Schilbach, E., Schultz, A.S.B., Scolnic, D., Strolger, L., Szalay, A., Seitz, S., Small, E., Smith, K.W., Soderblom, D.R., Taylor, P., Thomson, R., Taylor, A.N., Thakar, A.R., Thiel, J., Thilker, D., Unger, D., Urata, Y., Valenti, J., Wagner, J., Walder, T., Walter, F., Watters, S.P., Werner, S., Wood-Vasey, W.M., Wyse, R., 2016. The Pan-STARRS1 Surveys. *arXiv e-prints*, arXiv:1612.05560doi:[10.48550/arXiv.1612.05560](https://doi.org/10.48550/arXiv.1612.05560), [arXiv:1612.05560](https://arxiv.org/abs/1612.05560).
- Cochran, A.L., Levison, H.F., Stern, S.A., Duncan, M.J., 1995. The Discovery of Halley-sized Kuiper Belt Objects Using the Hubble Space Telescope. *ApJ* 455, 342. doi:[10.1086/176581](https://doi.org/10.1086/176581), [arXiv:astro-ph/9509100](https://arxiv.org/abs/astro-ph/9509100).
- Drake, A.J., Djorgovski, S.G., Mahabal, A., Beshore, E., Larson, S., Graham, M.J., Williams, R., Christensen, E., Catelan, M., Boattini, A., Gibbs, A., Hill, R., Kowalski, R., 2009. First Results from the Catalina Real-Time Transient Survey. *ApJ* 696, 870–884. doi:[10.1088/0004-637X/696/1/870](https://doi.org/10.1088/0004-637X/696/1/870), [arXiv:0809.1394](https://arxiv.org/abs/0809.1394).
- Flewelling, H.A., Magnier, E.A., Chambers, K.C., Heasley, J.N., Holmberg, C., Huber, M.E., Sweeney, W., Waters, C.Z., Calamida, A., Casertano, S., Chen, X., Farrow, D., Hasinger, G., Henderson, R., Long, K.S., Metcalfe, N., Narayan, G., Nieto-Santesteban, M.A., Norberg, P., Rest, A., Saglia, R.P., Szalay, A., Thakar, A.R., Tonry, J.L., Valenti, J., Werner, S., White, R., Denneau, L., Draper, P.W., Hodapp, K.W., Jedicke, R., Kaiser, N., Kudritzki, R.P., Price, P.A., Wainscoat, R.J., Chastel, S., McLean, B., Postman, M., Shiao, B., 2020. The Pan-STARRS1 Database and Data Products. *ApJS* 251, 7. doi:[10.3847/1538-4365/abb82d](https://doi.org/10.3847/1538-4365/abb82d), [arXiv:1612.05243](https://arxiv.org/abs/1612.05243).
- Fraser, W.C., Kavelaars, J.J., 2009. The Size Distribution of Kuiper Belt Objects for D gsim 10 km. *AJ* 137, 72–82. doi:[10.1088/0004-6256/137/1/72](https://doi.org/10.1088/0004-6256/137/1/72), [arXiv:0810.2296](https://arxiv.org/abs/0810.2296).
- Gaia Collaboration, Prusti, T., de Bruijne, J.H.J., Brown, A.G.A., Vallenari, A., Babusiaux, C., Bailer-Jones, C.A.L., Bastian, U., Biermann, M., Evans, D.W., Eyer, L., Jansen, F., Jordi, C., Klioner, S.A., Lammas, U., Lindgren, L., Luri, X., Mignard, F., Milligan, D.J., Panem, C., Poinson, V., Pourbaix, D., Randich, S., Sarri, G., Sartoretti, P., Siddiqui, H.I., Soubiran, C., Valette, V., van Leeuwen, F., Walton, N.A., Aerts, C., Arenou, F., Cropper, M., Drimmel, R., Høg, E., Katz, D., Lattanzi, M.G., O’Mullane, W., Grebel, E.K., Holland, A.D., Huc, C., Passot, X., Bramante, L., Cacciari, C., Castañeda, J., Chaoul, L., Cheek, N., De Angeli, F., Fabricius, C., Guerra, R., Hernández, J., Jean-Antoine-Piccolo, A., Masana, E., Messineo, R., Mowlavi, N., Nienartowicz, K., Ordóñez-Blanco, D., Panuzzo, P., Portell, J., Richards, P.J., Riello, M., Seabroke, G.M., Tanga, P., Thévenin, F., Torra, J., Els, S.G., Gracia-Abril, G., Comoretto, G., Garcia-Reinaldos, M., Lock, T., Mercier, E., Altmann, M., Andrae, R., Astraatmadja, T.L., Bellas-Velidis, I., Benson, K., Berthier, J., Blomme, R., Busso, G., Carry, B., Cellino, A., Clementini, G., Cowell, S., Creevey, O., Cuypers, J., Davidson, M., De Ridder, J., de Torres, A., Delchambre, L., Dell’Oro, A., Ducourant, C., Frémat, Y., García-Torres, M., Gosset, E., Halbwachs, J.L., Hambly, N.C., Harrison, D.L., Hauser, M., Hestroffer, D., Hodgkin, S.T., Huckle, H.E., Hutton, A., Jasiewicz, G., Jordan, S., Kontizas, M., Korn, A.J., Lanzafame, A.C., Mantega, M., Moitinho, A., Muinonen, K., Osinde, J., Pancino, E., Pauwels, T., Petit, J.M., Recio-Blanco, A., Robin, A.C., Sarro, L.M., Siopis, C., Smith, M., Smith, K.W., Sozzetti, A., Thuillot, W., van Reeven, W., Viala, Y., Abbas, U., Abreu Aramburu, A., Accart, S., Aguado, J.J., Allan, P.M., Allasia, W., Altavilla, G., Álvarez, M.A., Alves, J., Anderson, R.I., Andrei, A.H., Anglada Varela, E., Antiche, E., Antoja, T., Antón, S., Arcay, B., Atzei, A., Ayache, L., Bach, N., Baker, S.G., Balaguer-Núñez, L., Barache, C., Barata, C., Barbier, A., Barblan, F., Baroni, M., Barrado y Navascués, D.,

- Barros, M., Barstow, M.A., Becciani, U., Bellazzini, M., Bellei, G., Bello García, A., Belokurov, V., Bendjoya, P., Berihuete, A., Bianchi, L., Bienaymé, O., Billebaud, F., Blagorodnova, N., Blanco-Cuaresma, S., Boch, T., Bombrun, A., Borrachero, R., Bouquillon, S., Bourda, G., Bouy, H., Bragaglia, A., Breddels, M.A., Brouillet, N., Brüsemeister, T., Buccionelli, B., Budnik, F., Burgess, P., Burgon, R., Burlacu, A., Busonero, D., Buzzi, R., Caffau, E., Cambras, J., Campbell, H., Cancelliere, R., Cantat-Gaudin, T., Carlucci, T., Carrasco, J.M., Castellani, M., Charlot, P., Charnas, J., Charvet, P., Chassat, F., Chiavassa, A., Clotet, M., Cocozza, G., Collins, R.S., Collins, P., Costigan, G., 2016. The Gaia mission. *A&A* 595, A1. doi:10.1051/0004-6361/201629272, arXiv:1609.04153.
- Giorgini, J., 2011. Summary and status of the Horizons ephemeris system, in: Capitaine, N. (Ed.), *Journées Systèmes de Référence Spatio-temporels* 2010, pp. 87–87.
- Heinze, A., Egl, S., Juric, M., Moeyens, J., Jones, L., Sullivan, I., Bellm, E., 2022. Heliolinc3D: enabling asteroid discovery for the Legacy Survey of Space and Time (LSST), in: *AAS/Division for Planetary Sciences Meeting Abstracts*, p. 504.04.
- Heinze, A.N., Metchev, S., Trollo, J., 2015. Digital Tracking Observations Can Discover Asteroids 10 Times Fainter Than Conventional Searches. *AJ* 150, 125. doi:10.1088/0004-6256/150/4/125, arXiv:1508.01599.
- Heinze, A.N., Trollo, J., Metchev, S., 2019. The Flux Distribution and Sky Density of 25th Magnitude Main Belt Asteroids. *AJ* 158, 232. doi:10.3847/1538-3881/ab48fa, arXiv:1910.13015.
- Huang, Y., Cheng, Y., Bapna, A., Firat, O., Chen, D., Chen, M., Lee, H., Ngiam, J., Le, Q.V., Wu, Y., et al., 2019. Gpipe: Efficient training of giant neural networks using pipeline parallelism. *Advances in neural information processing systems* 32.
- Ivezić, v., Tyson, J.A., Acosta, E., Allsman, R., Anderson, S.F., Andrew, J., Angel, J.R.P., Axelrod, T.S., Barr, J.D., Becker, A.C., et al., 2008. Lsst: from science drivers to reference design and anticipated data products arXiv:0805.2366v4.
- Jurić, M., Kantor, J., Lim, K., Lupton, R.H., Dubois-Felsmann, G., Jenness, T., Axelrod, T.S., Aleksić, J., Allsman, R.A., AlSayyad, Y., Alt, J., Armstrong, R., Basney, J., Becker, A.C., Becla, J., Bickerton, S.J., Biswas, R., Bosch, J., Boutigny, D., Carrasco Kind, M., Ciardi, D.R., Connolly, A.J., Daniel, S.F., Daus, G.E., Economou, F., Chiang, H.F., Fausti, A., Fisher-Levine, M., Freemon, D.M., Gee, P., Gris, P., Hernandez, F., Hoblitt, J., Ivezić, Ž., Jammes, F., Jevremović, D., Jones, R.L., Bryce Kalmbach, J., Kasliwal, V.P., Krughoff, K.S., Lang, D., Lurie, J., Lust, N.B., Mullally, F., MacArthur, L.A., Melchior, P., Moeyens, J., Nidever, D.L., Owen, R., Parejko, J.K., Peterson, J.M., Petravicz, D., Pietrowicz, S.R., Price, P.A., Reiss, D.J., Shaw, R.A., Sick, J., Slater, C.T., Strauss, M.A., Sullivan, I.S., Swinbank, J.D., Van Dyk, S., Vujčić, V., Withers, A., Yoachim, P., LSST Project, f.t., 2015. The LSST Data Management System. *ArXiv e-prints* arXiv:1512.07914.
- Leclerc, G., Ilyas, A., Engstrom, L., Park, S.M., Salman, H., Madry, A., 2023. Ffcv: Accelerating training by removing data bottlenecks, in: *Proceedings of the IEEE/CVF Conference on Computer Vision and Pattern Recognition (CVPR)*, pp. 12011–12020.
- Lifset, N., Golovich, N., Green, E., Armstrong, R., Yeager, T., 2021. A Search for L4 Earth Trojan Asteroids Using a Novel Track-before-detect Multiepoch Pipeline. *AJ* 161, 282. doi:10.3847/1538-3881/abf7af, arXiv:2102.09059.
- Masci, F.J., Laher, R.R., Rusholme, B., Shupe, D.L., Groom, S., Surace, J., Jackson, E., Monkewitz, S., Beck, R., Flynn, D., Terek, S., Landry, W., Hacopians, E., Desai, V., Howell, J., Brooke, T., Imel, D., Wachter, S., Ye, Q.Z., Lin, H.W., Cenko, S.B., Cunningham, V., Rebbapragada, U., Bue, B., Miller, A.A., Mahabal, A., Bellm, E.C., Patterson, M.T., Jurić, M., Golkhou, V.Z., Ofek, E.O., Walters, R., Graham, M., Kasliwal, M.M., Dekany, R.G., Kupfer, T., Burdge, K., Cannella, C.B., Barlow, T., Van Sistine, A., Giomi, M., Fremling, C., Blagorodnova, N., Levitan, D., Riddle, R., Smith, R.M., Helou, G., Prince, T.A., Kulkarni, S.R., 2019. The Zwicky Transient Facility: Data Processing, Products, and Archive. *PASP* 131, 018003. doi:10.1088/1538-3873/aae8ac, arXiv:1902.01872.
- Mohan, J., Phanishayee, A., Raniwala, A., Chidambaram, V., 2020. Analyzing and mitigating data stalls in dnn training. *arXiv preprint arXiv:2007.06775*.
- Morbideilli, A., Nesvorny, D., Bottke, W.F., Marchi, S., 2021. A re-assessment of the Kuiper belt size distribution for sub-kilometer objects, revealing collisional equilibrium at small sizes. *Icarus* 356, 114256. doi:10.1016/j.icarus.2020.114256, arXiv:2012.03823.
- Pence, W., Seaman, R., White, R., 2011. Fpack and Funpack User's Guide: FITS Image Compression Utilities. *arXiv e-prints*, arXiv:1112.2671doi:10.48550/arXiv.1112.2671, arXiv:1112.2671.
- Schlaflly, E., Yeager, T., Pruet, K., Schneider, M., Ebert, J., Merl, D., Lifset, N., Armstrong, R., Dawson, W., Meyers, J., Perloff, A., Golovich, N., 2023. Space situational awareness for python. [Computer Software] <https://doi.org/10.11578/dc.20240417.1>. URL: <https://doi.org/10.11578/dc.20240417.1>, doi:10.11578/dc.20240417.1.
- Shao, M., Nemat, B., Zhai, C., Turyshv, S.G., Sandhu, J., Hallinan, G., Harding, L.K., 2014. Finding Very Small Near-Earth Asteroids using Synthetic Tracking. *ApJ* 782, 1. doi:10.1088/0004-637X/782/1/1, arXiv:1309.3248.
- Steil, T., Reza, T., Priest, B., Pearce, R., 2023. Embracing irregular parallelism in hpc with ygm, in: *Proceedings of the International Conference for High Performance Computing, Networking, Storage and Analysis*, Association for Computing Machinery, New York, NY, USA. URL: <https://doi.org/10.1145/3581784.3607103>, doi:10.1145/3581784.3607103.
- Thomas, J., 2024. Lawrence Livermore National Laboratorys El Capitan verified as world's fastest supercomputer. <https://www.llnl.gov/article/52061/lawrence-livermore-national-laboratorys-el-capitan-verified-worlds-fastest-supercomputer>.
- Tonry, J.L., Denneau, L., Heinze, A.N., Stalder, B., Smith, K.W., Smartt, S.J., Stubbs, C.W., Weiland, H.J., Rest, A., 2018. ATLAS: A High-cadence All-sky Survey System. *PASP* 130, 064505. doi:10.1088/1538-3873/aabadf, arXiv:1802.00879.
- Tyson, J.A., Guhathakurta, P., Bernstein, G.M., Hut, P., 1992. Limits on the Surface Density of Faint Kuiper Belt Objects, in: *American Astronomical Society Meeting Abstracts*, p. 06.10.
- Van Essen, B., Hsieh, H., Ames, S., Gokhale, M., 2012. Di-mmap: A high performance memory-map runtime for data-intensive applications, in: *2012 SC Companion: High Performance Computing, Networking, Storage and Analysis*, pp. 731–735. doi:10.1109/SC.Companion.2012.99.
- Wang, F., Yang, C.Q., Du, Y.F., Chen, J., Yi, H.Z., Xu, W.X., 2011. Optimizing linpack benchmark on gpu-accelerated petascale supercomputer. *Journal of Computer Science and Technology* 26, 854–865.
- Wells, D.C., Greisen, E.W., Harten, R.H., 1981. FITS - a Flexible Image Transport System. *AAPS* 44, 363.
- Whidden, P.J., Bryce Kalmbach, J., Connolly, A.J., Jones, R.L., Smotherman, H., Bektesevic, D., Slater, C., Becker, A.C., Ivezić, Ž., Jurić, M., Bolin, B., Moeyens, J., Förster, F., Golkhou, V.Z., 2019. Fast Algorithms for Slow Moving Asteroids: Constraints on the Distribution of Kuiper Belt Objects. *AJ* 157, 119. doi:10.3847/1538-3881/aafd2d, arXiv:1901.02492.
- Yeager, T., Pruet, K., Schneider, M., 2023. Long-term N-body Stability in Cis-lunar Space, in: Ryan, S. (Ed.), *Proceedings of the Advanced Maui Optical and Space Surveillance (AMOS) Technologies Conference*, p. 208.
- Zhai, C., Shao, M., Nemat, B., Werne, T., Zhou, H., Turyshv, S.G., Sandhu, J., Hallinan, G., Harding, L.K., 2014. Detection of a Faint Fast-moving Near-Earth Asteroid Using the Synthetic Tracking Technique. *ApJ* 792, 60. doi:10.1088/0004-637X/792/1/60, arXiv:1403.4353.
- Zhai, C., Shao, M., Saini, N.S., Sandhu, J.S., Owen, W.M., Choi, P., Werne, T.A., Ely, T.A., Lazio, J., Martin-Mur, T.J., Preston, R.A., Turyshv, S.G., Mitchell, A.W., Nazli, K., Cui, I., Mochama, R.M., 2018. Accurate Ground-based Near-Earth-Asteroid Astrometry Using Synthetic Tracking. *AJ* 156, 65. doi:10.3847/1538-3881/aacb28, arXiv:1805.01107.
- Zhai, C., Ye, Q., Shao, M., Trahan, R., Saini, N.S., Shen, J., Prince, T.A., Bellm, E.C., Graham, M.J., Helou, G., Kulkarni, S.R., Kupfer, T., Laher, R.R., Mahabal, A., Masci, F.J., Rusholme, B., Rosnet, P., Shupe, D.L., 2020. Synthetic Tracking Using ZTF Deep Drilling Data Sets. *PASP* 132, 064502. doi:10.1088/1538-3873/ab828b, arXiv:1907.11299.